RESEARCH ARTICLE

Novel eco-friendly electrospun nanomagnetic zinc oxide hybridized PVA/alginate/chitosan nanofibers for enhanced phenol decontamination

Marwa Elkady[1,2] · Eslam Salama[3,4] · Wael A. Amer[3] · El-Zeiny M. Ebeid[3] · Mohamad M. Ayad[3,5] · Hassan Shokry[6,7]

Abstract
In the current study, poly(vinyl alcohol)/alginate/chitosan (PVA/Alg/CS) composite nanofiber was immobilized with six different ratios of nanomagnetic zinc oxide (M-ZnO) (0 wt%, 0.2 wt%, 0.4 wt%, 0.6 wt%, 0.8 wt%, and 1 wt%) via the electrospinning technique. The various fabricated composite (M-6) nanofibers were characterized using Fourier transform infrared (FTIR), X-ray diffractometer (XRD), vibrating sample magnetometer (VSM), scanning electron microscope (SEM), atomic force microscope (AFM), thermogravimetric analysis (TGA), mechanical testing machine, and optical contact angle measurement. The fabricated composite nanofibers were applied for the adsorption of phenol from aqueous solutions. The 1.0 wt% M-ZnO/PVA/Alg/CS composite nanofibers were selected as the best phenol adsorbent with removal percentage of 84.22%. The influence of different processing parameter such as contact time, composite nanofiber dosage, pH, initial pollutant concentration, and temperature were examined. Increasing nanofiber dosage and the solution temperature was found to enhance the phenol adsorption onto the prepared nanocomposites. The maximum percentage of phenol removal was achieved at 84.22% after 90 min. Meanwhile, the maximum monolayer adsorption capacity (at pH = 5.0) was estimated to be 10.03 mg g^{-1} at 25 °C. Kinetic, isotherm, and thermodynamic studies were designated to proof the endothermic, spontaneous, and thermodynamically nature of the phenol adsorption process. These outcomes indicate the effectiveness of the fabricated M-ZnO/PVA/Alg/CS nanofibers as adsorbent materials for phenol from aqueous solutions.

Keywords Nanomagnetic ZnO composite · Polymeric hybrid nanofiber · Electrospinning · Phenol removal · Adsorption · Kinetics

✉ Hassan Shokry
  hassan.shokry@gmail.com

1 Fabrication Technology Research Department, Advanced Technology and New Materials Research Institute (ATNMRI), City of Scientific Research and Technological Applications (SRTA-City), New Borg El-Arab City, Alexandria 21934, Egypt

2 Chemical and Petrochemical Engineering Department, Egypt-Japan University of Science and Technology (E-JUST), New Borg El-Arab City, Alexandria 21934, Egypt

3 Chemistry Department, Faculty of Science, Tanta University, Tanta 31527, Egypt

4 Environment and Natural Materials Research Institute (ENMRI), City of Scientific Research and Technological Applications, New Borg El-Arab City, Alexandria 21934, Egypt

5 Institute of Basic and Applied Sciences, Egypt-Japan University of Science and Technology, New Borg El-Arab City, Alexandria 21934, Egypt

6 Electronic Materials Research Department, Advanced Technology and New Materials Research Institute (ATNMRI), City of Scientific Research and Technological Applications (SRTA-City), New Borg El-Arab City, Alexandria 21934, Egypt

7 Environmental Engineering Department, Egypt-Japan University of Science and Technology, New Borg El-Arab City, Alexandria 21934, Egypt

Introduction

Water is the foundation of all life on Earth. Water pollution becomes more and more serious trouble due to the fast-growing global population (Mekonnen and Hoekstra 2016; Pedro-Monzonís et al. 2015; Yin and Deng 2015). Phenolic pollutants are classified as one of the most serious hazardous pollutants in wastewater since they are harmful to organisms even at low concentrations. Discharging of phenol into the surface water, without treatment, leads to serious health risks to animals, humans, and the aquatic life systems. Hence, there is a persistent need to develop cost-effective technologies to extend water resources and to solve the problem of water pollution with phenol.

Recently, various treatment processes were introduced for the removal of phenol from wastewater such as distillation (El-Ashtoukhy et al. 2013), adsorption (Mukherjee and De 2014; Park et al. 2015), extraction (Rahmanian et al. 2014; Shokry et al. 2020), chemical oxidation (Du et al. 2012), ion exchange (Elkady et al. 2016a), electrochemical oxidation (Tasic et al. 2014), and biological treatment processes (Jalayeri et al. 2013). Among these techniques, the adsorption technique is considered the most extensively used route for wastewater treatment (Amer et al. 2018; Ayad et al. 2018). Many adsorbent materials were utilized for the phenol removal from wastewater. For instance, Shokry Hassan et al. (2017a) monitored the phenol removal from aqueous solutions in the presence of magnetic ZnO cellulose acetate composite nanofibers. However, Salari et al. (2019) investigated the phenol adsorption onto magnetic chitosan using genetic algorithm and surface methodology. In our previous study, magnetic ZnO nanotubes were fabricated via microwave technique toward phenol adsorption from aqueous solutions by batch experiments (Elkady et al. 2017). The fabricated nanomagnetic ZnO performed a relatively high adsorption efficiency which reached 87% within 90 min in the presence of 2 g/L of adsorbent material. Moreover, Babuponnusami and Muthukumar (2012) utilized nanozero valent iron for phenol removal by heterogeneous photo-electro-Fenton-like process. Similarly, Hayat et al. (2011) investigated the efficiency of different nano-ZnO samples which fabricated via the modified sol-gel method for phenol removal from water by heterogeneous photocatalytic process. Accordingly, polymeric nanofibrous membranes are currently one of the widest membrane type used for water treatment due to its higher flexibility and relatively low costs compared with the other membrane matrices (Yin and Deng 2015). Consequently, electrospinning technology is considered one of the most promising, efficient, and useful methods for fabrication of ultrathin fibers (Frenot and Chronakis 2003; Kimmer et al. 2009; Ramakrishna 2005). Electrospinning is a simple, great, cost-efficient, and multilateral technique to produce continuous ultrafine fibers from a wide range of materials involving composites, polymers, and

ceramics (Dersch et al. 2005; Jayaraman et al. 2004; Li and Xia 2004; Persano et al. 2013; Subbiah et al. 2005). This technique can be easily established in the laboratories as shown in Fig. 1 and also can be scaled upward to industrial processes (Ji et al. 2011). The nonwoven electrospun fibers have many advantages such as high surface area, small pore size, and high porosity as compared with regular fibers. These unique features make the nanofiber polymeric matrices to be good candidates for several applications including filtration, sensors, drug delivery, wound dressings, cosmetics, tissue engineering, energy conversion, and storage (Huang et al. 2003; Shokry Hassan et al. 2017b).

Many natural and synthetic polymer nanocomposites were employed for phenol decontamination from wastewater due to their suitable functional groups (Elkady and Shokry Hassan 2015; Yamasaki et al. 2006). Among the natural polymers, chitosan (CS) and alginate (Alg) are frequently used polysaccharides for bio-applications, where both these polymers can be produced from crustacean shell waste and brown seaweed (Anitha et al. 2014). CS is a linear cationic polysaccharide composed of β-(1,4)-linked-2-deoxy-2-amino-D-glucopyranose units and contains active amino and hydroxyl functional groups (Ayad et al. 2017a; b). Moreover, CS has many interesting properties such as biodegradability, biocompatibility, nontoxicity, hemostatic properties, antifungal, and antibacterial properties (Lee et al. 2009) and thus CS has been widely used in many applications such as biomedical and wastewater treatment. On the other hand, Alg is a natural hydrophilic anionic polymer, which has excellent biocompatibility, low toxicity, and capability to be used for pollutants removal from aqueous solutions (Sill and von Recum 2008). Furthermore, Alg polymer can improve the mechanical properties of the fabricated nanofibers, where it forms optically clear homogeneous blended nanofibers with PVA that enhances the tensile stress and Young modulus of the blended nanofibers compared with pure PVA (Islam and Karim 2010). Hence, there is a big challenge to form a uniform fiber without any beads in the presence of only CS and Alg. Thus, a high molecular weight polymeric material such as poly(vinyl alcohol) (PVA) is often added to increase the chain entanglement of polymers (Chang et al. 2012). The use of naturally based biopolymers such as CS as a cationic polysaccharide and Alg as an anionic polysaccharide attracted much attention due to their chemical stability, low price, high reactivity, and affinity for removal of various selected pollutants from wastewater (Barbusiński et al. 2016; Gokila et al. 2017; Nechita 2017; Ngo et al. 2015). For instance, Abdolmaleki et al. (2018) fabricated chitosan/PVA nanofibers by the electrospinning method and tested as an adsorbent for phenol decontamination. Moreover, Bahareh et al. (Alizadeh et al. 2018) used magnetic EDTA/CS/TiO$_2$ cross-linked nanocomposite for phenol and cadmium ( ) removal from wastewater. To the best of our knowledge, the electrospinning of

Fig. 1 The electrospinning technique to produce polymeric composite nanofibers
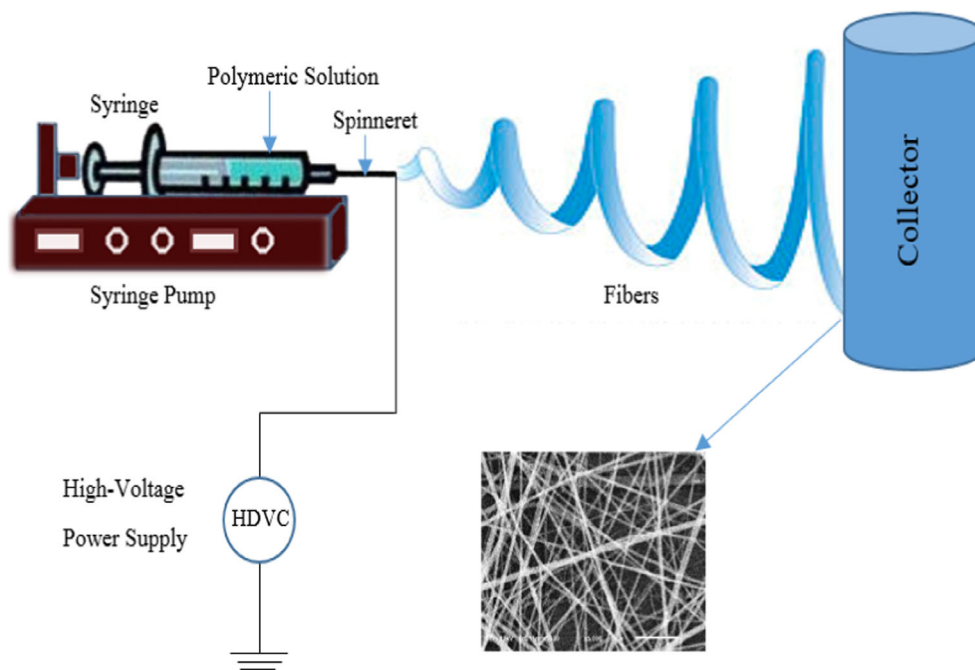
nanomagnetic ZnO immobilized with the three polymeric matrices (PVA, Alg, and CS) is lacking in the literature works. Moreover, the use of the formed composite nanofibers for phenol removal is missing. Therefore, the present work aims to perform a comparative study between the free PVA/Alg/CS composite nanofibers and nanomagnetic ZnO immobilized with PVA/Alg/CS composite nanofibers to get the maximum removal capacity toward phenolic compounds from aqueous solutions. Moreover, the influence of water treatment operation conditions on the adsorption process of phenol was investigated. Finally, the adsorption behavior and the reaction mechanism of phenol adsorption onto the optimum fabricated polymeric composite nanofibers were established.

Materials and methods

Materials

Poly(vinyl alcohol) 95.5–96.5%, with average molecular weight 85,000–124,000 g/mol, was purchased from Sigma-Aldrich (USA) and used without any further purification. Sodium alginate powder and aqueous glycerol were obtained from Universal Laboratories Pvt. Ltd. (Mumbai). CS of high molecular weight (~ 310,000 to > 375,000 Da) was supplied from Sigma-Aldrich (USA). Glacial acetic acid 99% (ADWIC, Egypt), glutaraldehyde (25% aqueous solution, ACROS Organics, USA), zinc acetate ($Zn(CH_3COO)_2 \cdot 2H_2O$, Rankem, Gurgaon, India), iron (III) chloride (Fisher Scientific, UK), iron (II) sulfate (Fisher Scientific, UK), phenol (LOBA Chemie, India), calcium chloride (Across

Organics, USA), sodium hydroxide (Sigma-Aldrich, Darmstadt, Germany), and absolute ethanol (Fisher Scientific, UK) were used as received.

Synthesis of zinc oxide nanotubes

Nanomagnetic zinc oxide was synthesized as described in our previous work (Elkady et al. 2017; Hafez et al. 2014). As a stabilizing agent, 25 mg of PVA was mixed with 14 mM of aqueous zinc acetate solution (150 mL), and sodium hydroxide was added dropwise for zinc salt reduction. The resulting solution was maintained in a microwave (THOMSON-COMBI1, Thomson Premier Lighting & Appliance, Logan, UT, USA) at 800 W for 1 h. The produced white powder was washed several times with absolute ethanol and distilled water to remove residual salts and then centrifuged at 4000 rpm. Finally, the resulting nano-ZnO was dried at 60 °C overnight.

Synthesis of nanomagnetic zinc oxide

For magnetite immobilization, 0.5 g of the synthesized zinc oxide nanotubes were suspended in 200 mL mixed solution of iron (III) chloride and iron (II) sulfate (with a molar ratio of 2:1) until a homogeneous suspension was obtained using a direct sonication probe ultrasonic homogenizer (Vibra-Cell VCX 500, SONICS, Newtown, CT, USA). Afterward, 5 M sodium hydroxide solution was added dropwise to the previous suspension at 70 °C and maintained for 30 min under constant stirring until black precipitate of magnetic zinc oxide appeared. Typically, the prepared black powder was washed several times with distilled water and absolute ethanol and

then separated via centrifugation at 4000 rpm. Finally, the prepared material was dried at 70 °C overnight.

Fabrication of nanomagnetic zinc oxide/PVA/Alg/CS polymeric composites

Poly(vinyl alcohol) (10 wt%) was dissolved in distilled water at 85 °C and kept under continuous stirring overnight. 1 wt% of Alg was prepared in 50%wt aqueous glycerol under stirring at 25 °C. Afterward, 1.5 wt% aqueous CS solution was prepared by dissolving CS powder in 5 wt% of aqueous acetic acid at 25 °C under stirring. Subsequently, the sodium Alg solution was added to PVA solution under magnetic stirring, and then the CS solution was added to the mixture solution in a PVA/Alg/CS volume ratio of 8:1:1. Finally, six concentrations of nanomagnetic zinc oxide (0.0 wt%, 0.2 wt%, 0.4 wt%, 0.6 wt%, 0.8 wt%, and 1.0 wt%) were added to the previous prepared polymeric solution under continuous stirring at 25 °C.

Electrospinning processes

The electrospinning process was done at room temperature (25 °C). The polymeric solutions were fed into the electrospinning system (NanoNc, Model: ESR100D, Republic of Korea). In this study, the optimum applied voltage was 23 kV. The distance between the needle tip and the collector was 14 cm with applied flow rate was 1 ml/h. The six resulted composite nanofibers (M-1, M-2, M-3, M-4, M-5, and M-6) with the different concentrations of nanomagnetic zinc oxide (0.0 wt%, 0.2 wt%, 0.4 wt%, 0.6 wt%, 0.8 wt%, and 1.0 wt%, respectively) were collected and dried at room temperature for further use.

Cross-linking of the fabricated composite nanofibers

The cross-linking step is required for hydrophilic polymers (PVA, Alg, and CS) to be useful in wastewater treatment applications without dissolving in water. In order to cross-link the Alg polymer, the fabricated fibers were immersed in 1% CaCl$_2$ ethanolic solution for 1 h and the resulting membranes were then treated with 10% glutaraldehyde vapor in a closed bottle for 24 h at 25 °C. After cross-linking, the membranes were washed out several times with pure methanol to eliminate any possible residual of glutaraldehyde and acids. Finally, the cross-linked composite nanofibers were soaked in distilled water for 24 h to confirm their water insolubility.

Characterization of the fabricated composite nanofibers

The fabricated M-6 composite nanofibers were characterized by Fourier transform infrared (FTIR) (Bruker, Bremen,

Germany), X-ray diffractometer (XRD) (Schimadzu-7000, Shimadzu Corporation, Kyoto, Japan), vibrating sample magnetometer (VSM) (Dexing, Model: 250, Lake Zurich, IL, USA), scanning electron microscopy (SEM) (JEOL JSM 6360LA, JEOL, Japan), (JEOL, JEM-2100, Japan with an accelerating voltage of 80 kV), atomic force microscopy (AFM) (Schimadzu SPM-9700, Japan), and thermogravimetric analysis (TGA) (Shimadzu TGA-50 instrument). Moreover, the Brunauer-Emmett-Teller (BET) surface area was examined via surface area analyzer (Beckman Coulter SA3100, Brea, CA, USA) by measurement of the N$_2$ adsorption-desorption isotherms at 77 K. All samples were degassed before measurements for 12 h under vacuum at 25 °C.

The tensile strength and elongation of the fabricated composite nanofibers were examined using a mechanical testing system (INSTRON-5500R, USA). To evaluate the surface hydrophilicity of the composite nanofibers, surface contact angles were measured using optical contact angle (OCA20, Data-physics Instruments GmbH, Germany).

Batch adsorption for phenol decontamination

The phenol adsorption efficiency of the prepared composite nanofibers (M-1, M-2, M-3, M-4, M-5, and M-6) with various immobilized magnetic ZnO ratios was investigated. Typically in the batch method, 20 mg of different composite nanofibers were mixed with 10 mL of constant phenol solution concentration of 10 mg/L of pH = 5 at room temperature using an orbital shaker (Yellow line, Germany) for 90 min. The residuals of the phenol were measured using UV-Vis spectrophotometer instrument (JASCO V-630) at wavelength $\lambda =$ 510 nm. The influence of different processing parameters such as contact time (0–180 min), solution pH (1–11), composite nanofiber dose (0.5–10 g/L), initial phenol concentration (0–100 ppm), and solution temperature (25–85 °C) on the adsorption process was examined. The removal percentage of phenol via the fabricated composite nanofibers was calculated from the following equation (Elkady et al. 2016a):

$$\text{Removal\%} = ((C_o - C_e)/C_o) \times 100 \tag{1}$$

where C_o is the initial phenol concentration (mg/L) and C_e is the phenol concentration at equilibrium in aqueous solution after phase separation (mg/L). The phenol adsorption capacity (mg/g) was determined from the following equation (Elkady et al. 2017):

$$q_e = V (C_o - C_e)/m \tag{2}$$

where q_e is the capacity of phenol adsorption (mg/g), V is the volume of phenol (L), and m is the mass of M-6 composite nanofibers (g). Moreover, the thermodynamic parameters were calculated, and the adsorption was evaluated using

Langmuir, Freundlich, and Temkin equilibrium isotherm models. Finally, the kinetics of the phenol adsorption process were examined using pseudo-first-order, pseudo-second-order, Elovich, and intraparticle diffusion models.

Results and discussions

Characterization of the synthesized composite nanofibers

Fourier transform infrared

FTIR spectrum of the fabricated M-6 composite nanofibers was compared with the spectrum of the prepared M-1 composite nanofibers in Fig. 2. The FTIR spectrum of M-1 composite nanofibers shows a broad band around 3400–3500 cm^{-1} due to the combination of stretching vibration of hydroxyl groups of polymeric matrices, and N-H_2 groups at CS (Ayad et al. 2014; Kumar et al. 2010; Siva Kumar et al. 2009). The band at 2925 cm^{-1} could be ascribed as the asymmetric stretching of CH_2 group of CS. Moreover, CS displayed characteristic band of CH_3 group and CH_3-O at 1028 cm^{-1} (Ayad et al. 2014; Liu et al. 2003). On the other hand, the antisymmetric carbonyl stretch band of Alg appears at 1629 cm^{-1}, while the symmetric carbonyl stretching vibration band is found at 1440 cm^{-1}.
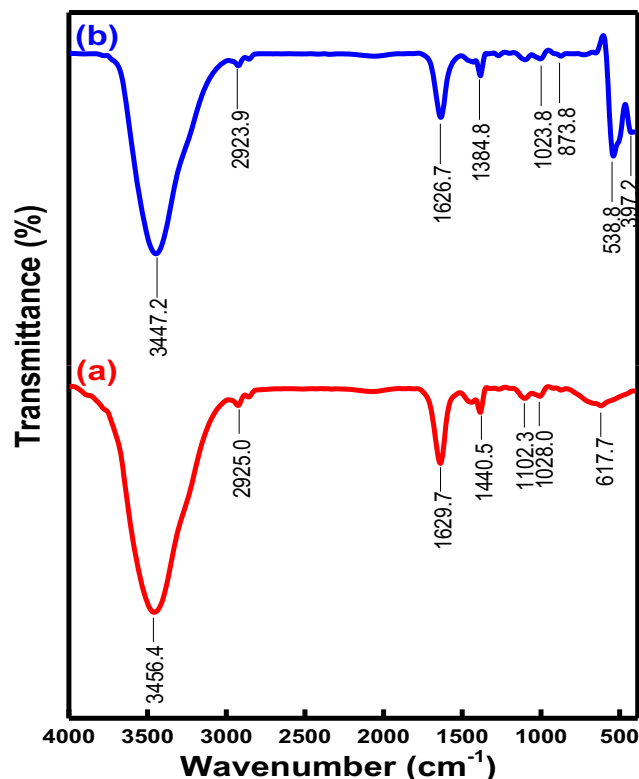
For the M-6 composite nanofibers, few bands were shifted to shorter wavenumbers that indicates the successful combination of the M-ZnO with polymeric matrices. For example, the bands at 3456, 2925, and 1629 cm^{-1} were shifted to 3447, 2923, and 1626 cm^{-1}, respectively. The bands at 1626 and 1384 cm^{-1} were corresponded to carbonyl and C-N stretching vibration at the polymeric matrix (Anžlovar et al. 2012; Kumar and Rani 2013; Shokry Hassan et al. 2017a). Moreover, the absorption band at 873 cm^{-1} is due to C-H rocking vibration at the polymeric matrix. The vibrational bands at 538 and 397 cm^{-1} are characteristic to the vibration of both magnetite and ZnO (Cornell and Schwertmann 2003; Zheng et al. 2011). These results indicated the successful incorporation of nano-M-ZnO into CS/Alg/PVA composite nanofibers (Ahmed et al. 2018). The slight change in characteristic peaks of CS, Alg, and PVA spectrum could be attributed to the uniform incorporation of M-ZnO nanotubes with the polymeric matrices (Gutha et al. 2017).

X-ray diffraction

The crystallinity degree of both M-1 and M-6 composite nanofibers are investigated as shown in Fig. 3a, b. The XRD patterns of the optimized M-1 composite nanofibers show abroad peak around 2θ of 20° which is corresponding to

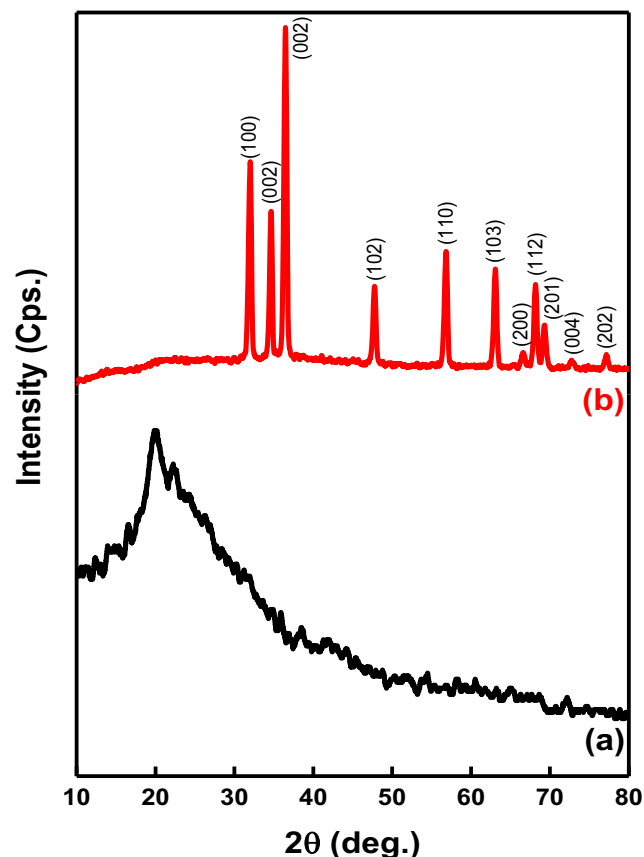Fig. 2 FTIR spectra of (a) M-1 and (b) M-6 composite nanofibers

Fig. 3 XRD patterns of (a) M-1 and (b) M-6 composite nanofibers

PVA (Alakanandana et al. 2016; Jiao et al. 2017; Voronova et al. 2015), Alg (Jana et al. 2015), and CS (Ayad et al. 2014; Jiao et al. 2017). Meanwhile, these XRD patterns confirm the lower crystallinity of the prepared composite nanofibers due to the presence of PVA and Alg (Karim 2013) that possess amorphous character (Shokry Hassan et al. 2017b; Voronova et al. 2015). Moreover, the crystalline peak of CS exhibited at 20.14° is assigned to the intra-molecular and inter-molecular hydrogen bonding between amino and hydroxyl groups, which lead to the linear accumulation of the structure chains (Ayad et al. 2014). On the other hand, the XRD patterns of M-ZnO (Fig. 3b) demonstrated that the all characteristic peaks at 2θ of 31.73, 34.38, 36.21, 47.48, 56.53, 62.77, 66.30, 67.86, 69.00, 72.45, and 76.86 of the synthesized nanomagnetic ZnO can be indexed to the wurtzite hexagonal structure with a high degree of crystallinity without any impurities (Pascariu et al. 2018). These results are in good agreement compared with the obtained values of ZnO reference card (JCPDS, card number 01-089-1397) (Kumaraswamy et al. 2017; Roy et al. 2013; Shokry Hassan et al. 2017b; Yang et al. 2004).

Vibrating sample magnetometer

The magnetic properties of the fabricated M-6 composite nanofibers were investigated at room temperature using a vibrating sample magnetometer. The hysteresis loop of the prepared M-6 composite nanofibers is shown in Fig. 4. It is observed that the fabricated nanofibers are a typical superparamagnetic material. The saturation moment per unit mass (Ms) of the synthesized M-6 composite was recorded 287.48 memu/g which is relatively lower than that of the magnetic nano-zinc oxide prepared at our pervious study (Elkady et al. 2017). The assigned data shows the low immobilization of magnetite nanoparticles into the polymeric membrane. Moreover, these results agree with previous studies showed
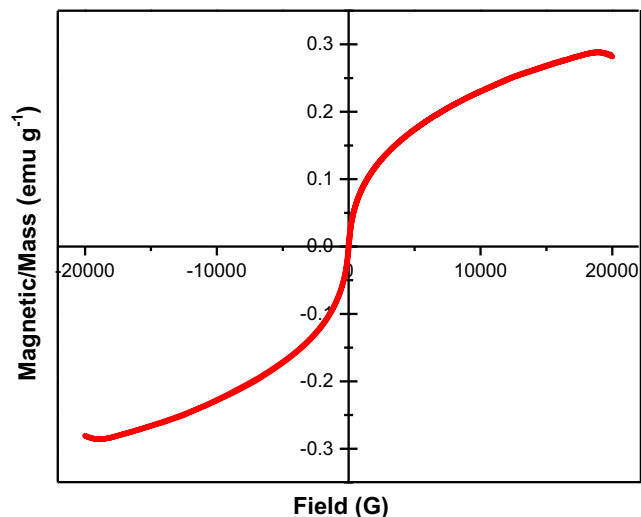

Fig. 4 Magnetization curves of M-6 composite nanofibers

that magnetite nanoparticles display superparamagnetic properties due to their particle size effect (Park et al. 2010; Shokry et al. 2020).

Scanning electron microscope

Scanning electron microscope analysis was used to investigate the surface morphological structure of PVA/Alg/CS-based nanofibers before and after nanomagnetic ZnO immobilization. From Fig. 5, it is demonstrated that the fabricated nanofibers have a uniform, homogenous, and ordered shape with acceptable average diameters of 235 ± 52 nm and 295 ± 65 nm for M-1 and M-6 composite nanofibers, respectively. This result confirms the successful fabrication of uniform polymeric composite nanofibers (Shokry Hassan et al. 2017a).

Atomic force microscope

AFM technique was used to demonstrate the three main properties of the surfaces of the fabricated fibers: surface morphology including pore size distribution, membrane adhesion (fouling), and surface electrical properties. The AFM images introduce the possibility of observing the surface topography. Figure S1 shows (a) 2D, (b) 3D, (c) phase AFM images of M-1 composite nanofibers, while Fig. S1 images (d), (e), and (f) characterize 2D, 3D, and phase of M-6 composite nanofibers. Comparing the AFM images indicated that the roughness increased from 0.24 μm for M-1 composite nanofibers to 1.35 μm for M-6 composite nanofibers. This increment of surface roughness may be returned to the increase in membrane hydrophobicity (Elkady et al. 2015).

BET surface area

The specific surface area of M-1 and M-6 composite nanofibers was 26.28 and 66.27 m^2/g, respectively, as shown in Fig. S2 (a, b). These results of the surface area are relatively high for material adsorption (Shokry et al. 2020; Sun and Uyama 2013; Wang et al. 2015). In addition, the total pore volume of M-1 and M-6 composite nanofiber membranes were 0.24 and 0.25 cm^3/g respectively. Furthermore, the mean pore diameters of the obtained composite nanofibers were 36.97 and 15.29 nm for the free and M-ZnO composite nanofibers, respectively. According to these results, the addition of M-ZnO has a positive impact on the surface area measurements. These data indicate that the fabricated composite nanofibers achieve significantly high surface area and porosity, which are very important for various potential applications (Elkady and Shokry Hassan 2015).

Fig. 5 SEM photographs of **a** M-1 and **b** M-6 composite nanofibers

(a)

(b)
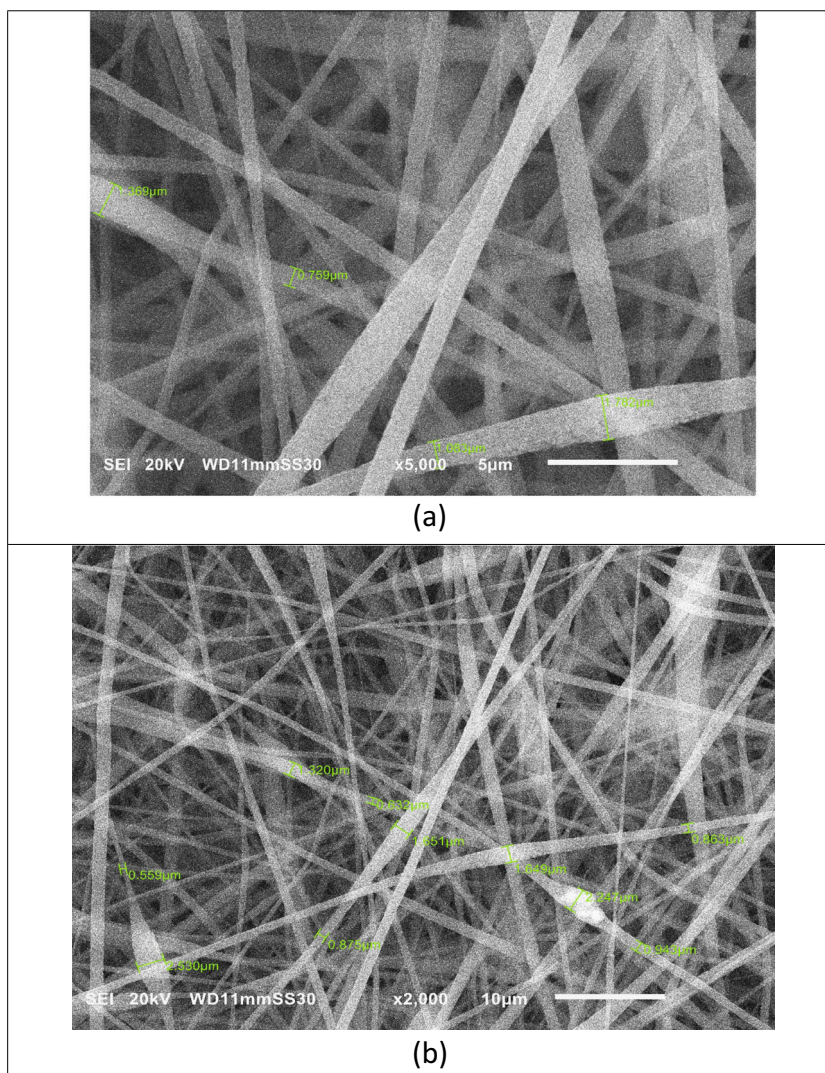
Thermogravimetric analysis

The thermograms of the M-1 and M-6 composite nanofibers are shown in Fig. 6. The TGA curves of the fabricated composite nanofibers indicate the presence of a weight loss stage of about 8% at 160 °C that can arises from the loss of water molecules (Shokry et al. 2020). The second weight loss stage positioned between 240 and 350 °C was about 40 wt% and this step can be assigned to the cleavage of side chain of the polymeric fiber (Liu et al. 2003). The third stage of weight loss ranged from 350 to 450 °C that attributed to the cleavage of nanofibers backbone (Elkady and Shokry Hassan 2015). Finally, the total weight loss step recorded about 99 wt% for M-1 membrane and about 89 wt% at 800 °C for M-6 composite nanofibers (Sargazi et al. 2019). From these results, both of the fabricated composite nanofibers were found to possess good thermal stability (Khan et al. 2018).
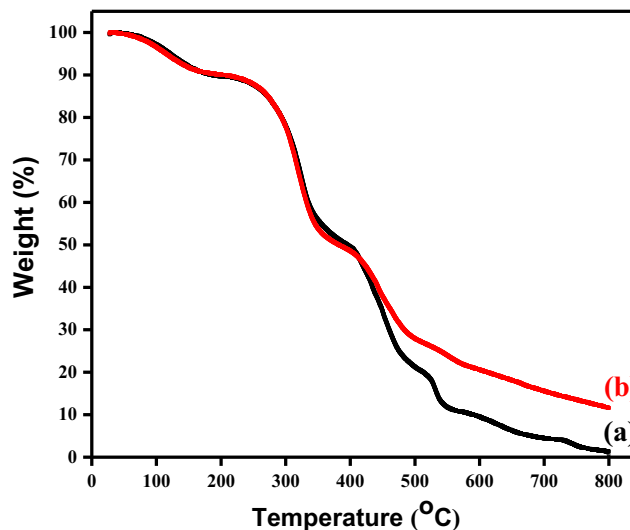

Fig. 6 TGA curves of (a) M-1 and (b) M-6 composite nanofibers

Tensile strength measurement

The mechanical tensile strength and elongation at break of the M-1 and M-6 composite nanofibers were carried out using the universal material testing machine. The extension rate and the clip distance were found to be 5 mm/min and 50 mm, respectively. As shown in Figs. S3 and S4, the tensile strength and elongation at break of the M-6 composite nanofibers were improved as compared with M-1 composite nanofibers as a result of nanomagnetic ZnO addition (Peña-Reyes et al. 2017). The highest tensile strength values were recorded at 11.08 and 9.43 N/mm^2 for M-6 and M-1 composite nanofibers, respectively.

Contact angle measurements

The contact angle was employed to characterize the relative hydrophilicity or hydrophobicity of the fabricated membrane surface as given in Tables S1 and S2. From Figs. S5 and S6, it is obvious that the immobilization of nanomagnetic ZnO into PVA/Alg/CS nanofibers positively influenced the contact angle values. Accordingly, the mean value of theta for M-1 composite nanofibers was recorded as 67.02 compared with 85.48 recorded for M-6 composite nanofibers. These results confirm the hydrophobicity character of the fabricated composite nanofibers particularly M-6 composite nanofibers (Ma et al. 2010; Zhao et al. 2011).

Application of the fabricated composite nanofibers for phenol removal

The feasibility of the prepared composite nanofibers with different immobilization M-ZnO ratios was examined for the adsorption of phenol from aqueous solutions at room temperature using the batch technique (Elkady et al. 2017). Figure 7 shows that the M-1 nanocomposite sample possessed the lowest phenol removal percentage of 37.65%. However, the M-6 nanocomposite sample was the best phenol adsorbent with a removal percentage of 84.22%; so, this sample was selected for the rest of study.

Influence of contact time on the phenol adsorption

The influence of contact time on the percentage of phenol adsorption onto sample M-6 nanocomposite was traced at different time intervals. As shown in Fig. 8, the phenol adsorption onto the fabricated composite nanofibers increased with increasing the contact time initially till reaching the equilibrium after 120 min. The high adsorption rate of phenol may be referred to the highly available surface area of the prepared composite nanofibers (El-Aassar et al. 2016; Shokry et al. 2020). The quantity of phenol adsorbed onto the composite nanofibers is at dynamic equilibrium with phenol ions
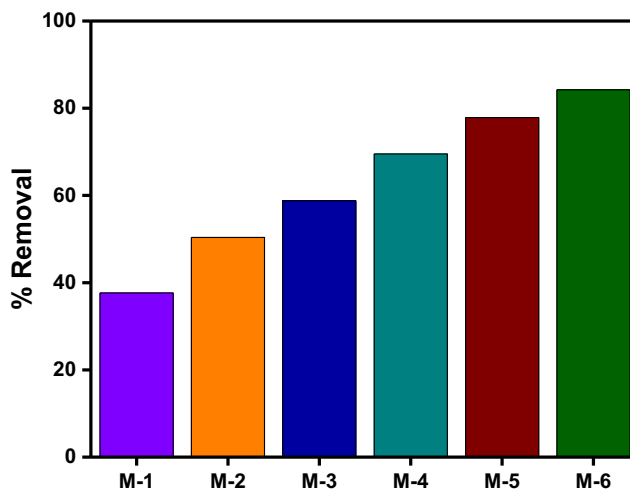
Fig. 7 Phenol removal by the fabricated composite nanofibers (contact time = 90 min, pH = 5, initial phenol concentration = 10 ppm, agitation speed = 440 rpm, composite nanofiber dosage = 2 g/L, and temperature = 25 °C)

desorbed from the polymeric composite nanofibers (Malayeri et al. 2014). The optimum contact time of the phenol adsorption process was recorded after 90 min, with a maximum phenol percentage removal of 84.22%. At the second stage of the adsorption process, the active sites of the M-6 composite nanofibers were saturated with the phenolic pollutants after the equilibrium (Mohy-Eldin et al. 2010) time.

Influence of M-6 composite nanofiber dosage on the phenol adsorption

The adsorbent dosage has a significant impact on the adsorption process because of its strong influence on the capacity of the adsorbent material at a given initial concentration of the pollutant (Elkady et al. 2018; Shokry et al. 2020). The
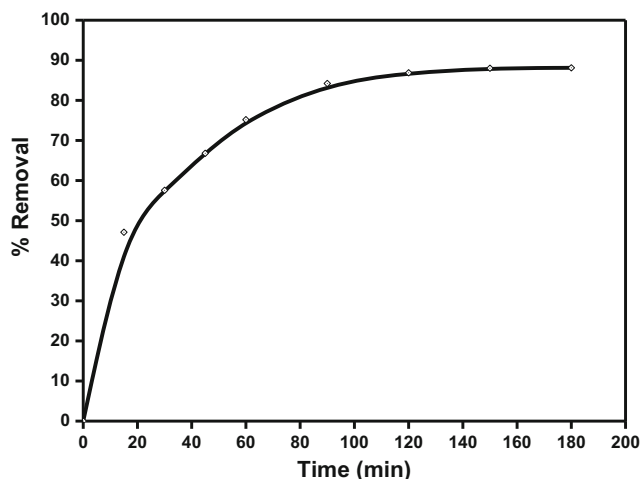
Fig. 8 Influence of contact time on phenol adsorption process onto M-6 composite nanofibers (pH = 5, initial phenol concentration = 10 ppm, agitation speed = 440 rpm, composite nanofiber dosage = 2 g/L, and temperature = 25 °C)

adsorbent dosage effect of M-6 composite nanofibers was investigated after 90 min. Figure 9 shows that the percentage of phenol removal was enhanced from 53.52 to 95.44% as M-6 composite nanofiber dosage increased from 0.5 to 20 g/L. However, a decrease in the adsorption capacity appeared with increasing of the composite nanofiber dosage. The decline of adsorption capacity at high material concentration may be attributed to the residual of the unsaturated adsorption sites onto the M-6 composite nanofibers (Vijayalakshmi et al. 2010). Moreover, the increase in the M-6 composite nanofiber dosage leads to the availability of more active sites for the phenol adsorption. These results may be due to the large determined active surface area of the fabricated M-6 composite nanofibers (Elkady et al. 2016a). Accordingly, the optimum dosage of M-6 composite nanofibers was achieved at 2 g/L, which represented to the economical dosage of the adsorption process.

Influence of initial pH on the phenol adsorption

The initial solution's pH represents an essential factor in the control of the phenol adsorption process onto the fabricated composite nanofibers. This parameter affects both the degree of ionization of phenol and the charge of the adsorbent material surface (Elkady et al. 2018). The effect was studied from pH 1 up to 11. It can be noticed from Fig. 10 that high adsorption capacity and removal percentage was achieved at low pH values, which demonstrates that M-6 composite nanofibers have high adsorption efficiency in the acidic medium. The adsorption percentage of phenol was found to be high till pH = 5 with 84.22% phenol removal and then the adsorption gradually declines with increasing of solution's pH with the lowest adsorption of 56% phenol removal at pH 11.
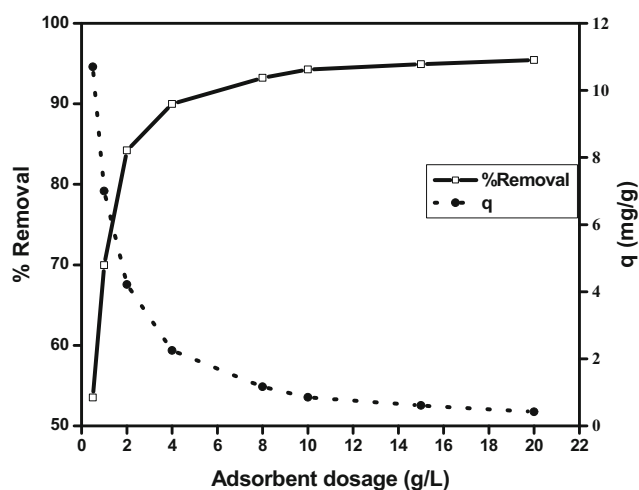

Fig. 10 Influence of solution pH on the percentage of phenol removal onto M-6 composite nanofibers (initial phenol concentration = 10 ppm, composite nanofiber dosage = 2 g/L, agitation speed = 440 rpm, contact time = 90 min, and temperature = 25 °C)

Therefore, pH = 5 was selected as optimum pH for the rest of the adsorption study onto the prepared M-6 composite nanofibers. The zero charge point (pzc) of the synthesized nanomagnetic ZnO was recorded at around 6 (Farrokhi et al. 2014). Accordingly, at pH < 6, the surface of the nanomagnetic ZnO is positively charged, so there is an electrostatic attraction between the positively charged surface of nanomagnetic ZnO and the unionized species of phenol (Parida and Pradhan 2010). Furthermore, as the solution's pH increases, the adsorbent surface became negatively charged, which results in reducing phenol adsorption due to the repulsive forces between the negatively charged magnetic ZnO surface and the phenolate ions. These results attributed to the pKa value of phenol around 9.8 (Han and Tao 2006).

Influence of initial phenol concentration on the adsorption process

The impact of phenol's initial concentration on the phenol decontamination process at equilibrium was achieved in the concentration range of 5 to 100 mg/L using 2 g/L of M-6 composite nanofibers at pH 5 for 90 min. Figure 11 demonstrates the enhancement in the adsorption capacity as the phenol initial concentration increased from 5 to 100 mg/L, which agrees with other reported studies (Elkady et al. 2017; Elkady et al. 2016a; Shokry Hassan et al. 2017a). This behavior may be due to the saturation of the active sites of the prepared M-6 composite nanofibers as the phenol concentration increased. From the previous results, it is clear that the fabricated M-6 composite nanofibers are effectively capable of removing phenol from aqueous solutions at various phenol concentrations; this behavior is due to the characteristic surface area of composite nanofiber that was estimated previously as 66.27 m^2/g.

Fig. 9 Influence of M-6 composite nanofiber dosage on both phenol percentage removal and phenol uptake capacity onto (contact time = 90 min, pH = 5, initial phenol concentration = 10 ppm, agitation speed = 440 rpm, and temperature = 25 °C)
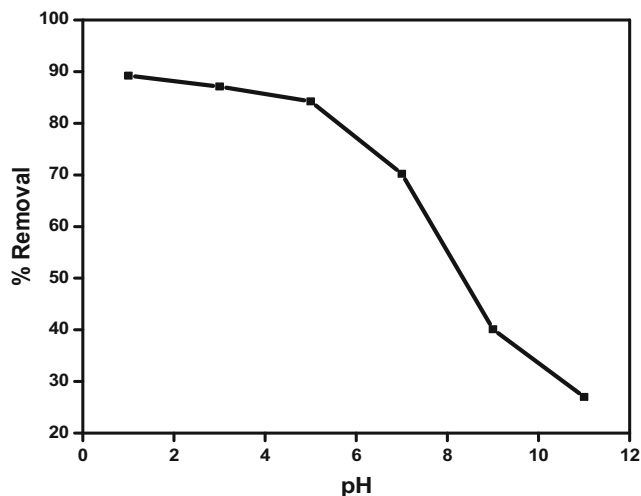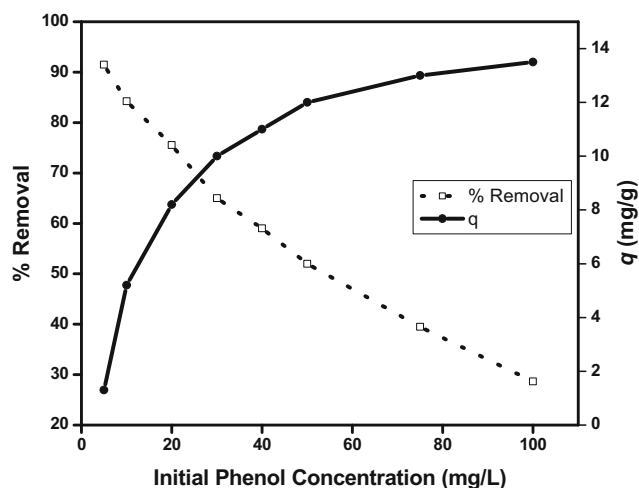
Fig. 11 Influence of initial phenol concentration on both the percentage of phenol removal and phenol uptake capacity onto M-6 composite nanofibers (pH = 5, composite nanofiber dosage = 2 g/L, agitation speed = 440 rpm, contact time = 90 min, and temperature = 25 °C)

Influence of solution temperature on the phenol adsorption

Figure 12 investigated the influence of the temperature on the phenol removal onto the fabricated M-6 composite nanofibers. The rising of solution temperature was found to increase the phenol adsorption process. This behavior arises from enhancing the rate of phenol diffusion into the pores of the fabricated M-6 composite nanofibers at higher temperatures due to the creation of new adsorption sites onto the M-6 composite nanofibers at high temperatures (Abd El-Latif and Elkady 2011; Shokry Hassan et al. 2015). According to these results, the phenol decontamination onto the M-6 composite nanofibers is an endothermic process (Elkady et al. 2017).
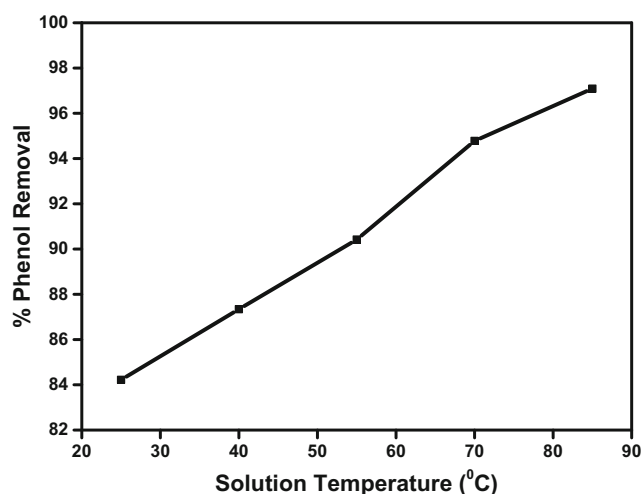
Thermodynamics and equilibrium modeling

The various thermodynamic parameters that should be considered to investigate any adsorption process are the changes in enthalpy ($\Delta H°$), standard free energy ($\Delta G°$), and entropy ($\Delta S°$). The value of the standard enthalpy and entropy can be calculated from the Van't Hoff equation as follows:

$$\ln K_c = \frac{\Delta S°}{R} - \frac{\Delta H°}{RT} \tag{3}$$

where the universal gas constant (R) = 8.314 J/mol K, T is the solution temperature in Kelvin while $K_c = F_e/(1 - F_e)$, and $F_e = (C_o - C_e)/C_o$ is the fraction adsorbed at equilibrium. Figure 13 indicated that the Van't Hoff plot of $\ln K_c$ against $1000/T$ gives a straight line with an acceptable value of correlation coefficient (R^2) at different investigated phenol concentrations. The values of $\Delta S°$ and $\Delta H°$ can be respectively calculated from the intercept and the slope of the Van't Hoff plot. Furthermore, the activation energy (E_a) can be determined from the following equation (Lu et al. 2016):

$$E_a = \Delta H° + RT \tag{4}$$

The values of $\Delta H°$, $\Delta G°$, $\Delta S°$, and E_a at different temperatures are listed in Table 1. The negative values of free energy changes $\Delta G°$ indicate the spontaneous and thermodynamically nature of the phenol adsorption process onto the fabricated M-6 composite nanofibers. Moreover, the calculated positive value of enthalpy indicates the endothermic in nature of the adsorption process. On the other hand, the positive value of entropy illustrates an increase in disorder at the solid/liquid interface during the phenol decontamination process (Thinakaran et al. 2008).

Fig. 12 Influence of phenol solution temperature on the percentage of phenol removal onto M-6 composite nanofibers (initial phenol concentration = 10 ppm, composite nanofiber dosage = 2 g/L, agitation speed = 440 rpm, contact time = 90 min, and pH = 5)
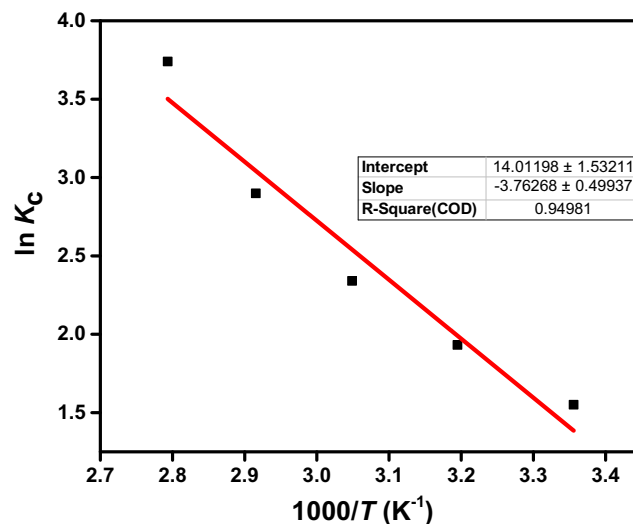

Fig. 13 The Van't Hoff plot of $\ln K_c$ against $1000/T$ for phenol adsorption onto M-6 composite nanofibers

Table 1 Thermodynamic parameters for phenol adsorption onto M-6 composite nanofibers

Temp. (K)	1000/T	C_{Be}	C_{Ae}	K_c	lnK_c	$\Delta G°$ (kJ/mol)	E_a (kJ/mol)	$\Delta H°$ (kJ/mol)	$\Delta S°$ (J/mol K)
298	3.36	8.25	1.75	4.71	1.55	−3.84	33.83	31.35	116.40
313	3.19	8.73	1.27	6.87	1.93	−5.02	33.95		
328	3.05	9.12	0.88	10.36	2.34	−6.38	34.08		
343	2.92	9.48	0.53	18.05	2.89	−8.25	34.20		
358	2.79	9.77	0.23	42.10	3.74	−11.13	34.33		

Equilibrium isotherm analysis for the phenol adsorption

The Langmuir, Freundlich, and Temkin isotherm models were applied to investigate the adsorption behavior and the reaction mechanism of phenol adsorption onto the fabricated M-6 polymeric composite nanofibers. The linearized plot of C_e/q_e versus C_e represented a straight line with a relative high correlation coefficient ($R^2 = 0.993$) (Elkady et al. 2016b):

$$\frac{C_e}{q_e} = \frac{1}{q_m K} + \frac{C_e}{q_m} \tag{5}$$

where q_e is the amount phenol adsorbed at equilibrium (mg/g), C_e is the equilibrium concentration of the adsorbate ions (mg/L), and q_m and K_L are Langmuir constants referred to the maximum monolayer adsorption capacity (mg/g) and adsorption energy (L/mg), respectively. According to the calculated parameters in Table 2 and Fig. S7, the Freundlich model is the best suitable model to describe the adsorption process of phenol onto the fabricated composite nanofibers. Moreover, the value of the separation factor (R_L) is 0.049, which falls in the range 0 to 1 that proves the favorable adsorption process description via the Langmuir model (Elkady et al. 2017; Üner et al. 2016). On the contrary, the best fit of the equilibrium data with the Freundlich isotherm assumes multilayer adsorption on heterogeneous surfaces (Üner et al. 2016). However, the adsorption intensity (n_F) calculated from the Freundlich model recorded 3.639 which is greater than unity, illustrating that the phenol adsorption process onto M-6 composite nanofibers is favorable (Üner et al. 2016). Therefore, the Freundlich isotherm is the best favorable model for representing the phenol adsorption process onto the prepared M-6 composite nanofibers, which supposes that the multilayer adsorption demonstrates the predictions about the physical adsorption of phenolic pollutants onto the fabricated

composite nanofibers (Elkady et al. 2018; Shokry Hassan 2019).

Comparison of adsorption capacity for prepared composite nanofibers with other adsorbent nanomaterials

To compare the adsorption performance of the prepared M-6 composite nanofibers with the other similar based nanomaterials, the monolayer adsorption capacities (q_m) were compared. Table 3 presents the comparable adsorption capacity of fabricated 1.0 wt% M-ZnO/PVA/Alg/CS composite nanofibers with that of the other adsorbent nanomaterials. Consequently, the fabricated M-6 composite nanofibers showed promising and appropriate results for phenol adsorption from aqueous solutions.

Kinetic models of phenol adsorption

To verify the adsorption mechanism of phenolic compounds from aqueous solution onto the fabricated M-6 composite nanofibers, the kinetics of the adsorption process were studied by applying the theoretical modeling of pseudo-first-order, pseudo-second-order, Elovich, and intraparticle diffusion models. The Lagergren first order is represented by the following equation (Alkaram et al. 2009):

$$\ln(q_e - q_t) = \ln q_e - k_1 t \tag{6}$$

where q_e and q_t are the amounts of phenol adsorbed ions (mg/g) at equilibrium and at time t (min), respectively. k_1 (min) is the rate constant of the first-order reaction. Furthermore, the phenol adsorption kinetic data were investigated using the pseudo-second-order kinetic model that can be expressed by:

$$t/q_t = (1/k_2 q^2) + t/q \tag{7}$$

Table 2 Isotherm parameters of Langmuir, Freundlich, and Temkin models for phenol removal onto M-6 composite nanofibers

Langmuir parameters			Freundlich parameters			Temkin parameters		
q_m (mg/g)	K_L (L/mg)	R^2	K_F (mg/g)	n_F	R^2	A (L/g)	B (J/mo)	R^2
10.030	0.196	0.993	0.475	3.639	0.997	6.478	1.513	0.923

Table 3 Comparison of calculated monolayer adsorption capacity for different adsorbent nanomaterials

Adsorbent material	General conditions	Adsorption capacity (mg/g)	Reference
M-6 composite nanofibers	1wt % M-ZnO/10% wt/v PVA/1% wt/v Alg/1.5% wt/v CS	10.03	Present study
Magnetic ZnO nanotubes	Fabricated via microwave technology followed by sonic precipitation of magnetite nanoparticles	20.40	Elkady et al. (2017)
Chitosan/PVA/zerovalent iron nanofibers	Biopolymeric synthesized chitosan/PVA/zerovalent iron nanofibers	1.68	Chauhan et al. (2014)
Magenetite reduced graphene oxide composite	Water-dispersible magnetite/graphene hybrids fabricated using chemical reaction	5.83	Chandra et al. (2010)
Porous $CS/Fe_3O_4/Fe(OH)_3$ microsphere	Prepared iron-doped chitosan and iron-coated chitosan flakes	8.47	Gupta et al. (2009)
Chitosan beads	Reaction time = 24 h, PH = 5, and reaction temp. = 25 °C	1.83	Chen and Chung (2006)
Chitosan/MWCNT/Fe_3O_4	Chitosan/MWCNT/Fe_3O_4 composite nanofiber was fabricated via electrospinning process	6.45	Beheshti et al. (2016)
Chitosan/graphene oxide composite nanofiber	Electrospun chitosan/graphene oxide (GO) nanofiber were synthesized using electrospinning process.	5.50	Najafabadi et al. (2015)

where k_2 is the equilibrium constant of the second-order reaction rate (g/mg min). The Elovich equation was demonstrated for the multilayer adsorption as follows:

$$q_t = \alpha + \beta \ln t \qquad (8)$$

where α signifies the initial adsorption rate (mg/g min) and β is correlated to the surface coverage degree and physical adsorption activation energy (g/mg). The constants α and β can be calculated from the slope and intercept of the linear plot of q_t versus $\ln t$. Finally, the possibility of the intraparticle diffusion affecting the adsorption process was applied by Weber and Morris (Elkady et al. 2017; Shokry et al. 2020) using the intraparticle diffusion model from the following equation:

$$q_t = k_i t^{1/2} + C \qquad (9)$$

where k_i is the constant of the intraparticle diffusion rate.

The linearity of t/q_t versus time with high correlation coefficient value ($R^2 = 0.999$) illustrates that the adsorption process of phenol follows the second-order rate kinetic model as shown in Table 4 and Fig. S8 (Elkady and Shokry Hassan 2015). Moreover, the experimentally measured value (4.211) of q_e of pseudo-second order is very close to the estimated value (4.593). However, the intraparticle diffusion model was given two separate regions. These two regions suggest that the adsorption process contains both surface adsorption and intraparticle diffusion. The intraparticle diffusion constant (k_i) and the value of C were separately calculated from the slope and intercept of the two linear regions as listed in Table 4. Additionally, the values of C give prediction about the thickness of the boundary layer. It is clear from Table 4 that the thickness of the boundary layer of the second region, which referred to the intraparticle diffusion (C_2), is larger than

the thickness of the boundary layer of the first region, which corresponds to the film diffusion (C_1). Consequently, the value of the intraparticle diffusion constant (k_{i2}) is lower than the film diffusion constant (k_{i1}). These results give prediction that the sorption process was controlled mainly by intraparticle diffusion (Namasivayam and Sureshkumar 2008). According to these results, the pseudo-second-order and intraparticle diffusion kinetic models are considered the most fitted for describing the phenol adsorption process onto the fabricated M-

Table 4 Pseudo-first-order, pseudo-second-order, Elovich, and intraparticle diffusion kinetic parameters for phenol removal onto M-6 composite nanofibers

Kinetic model	Parameter	Value
Pseudo-first order	$q_{exp.}$ (mg/g)	4.211
	q_{theor} (mg/g)	3.265
	K_1 (min^{-1})	0.032
	R^2	0.979
Pseudo-second order	q_{exp} (mg/g)	4.211
	q_{theor} (mg/g)	4.593
	K_2 (g/mg min)	0.024
	R^2	0.999
Elovich kinetic model	α (mg/g min)	− 0.264
	β (g/mg)	0.955
	R^2	0.981
Intraparticle diffusion kinetic model	C_1 (mg/g min)	0.992
	C_2 (mg/g min)	1.883
	k_{i1} (g/mg)	0.3332
	k_{i2} (g/mg)	0.2574
	R^2	0.992

6 composite nanofibers that confirms the physical adsorption process (Abd El-Latif and Elkady 2011).

Regeneration of M-ZnO/PVA/Alg/CS composite nanofibers

The regeneration test of the adsorbent material is considered the most significant factor because it touches on the overall cost in the real applications (Elzain et al. 2019). From all of the elution reagents, sodium hydroxide is considered the most favorable for phenol desorption (Ozkaya 2007). Consequently, to investigate the regeneration process, the final centrifuged form of M-6 composite nanofibers was washed several times with distilled water and then soaked into 0.2 N sodium hydroxide for 4 h under continuous stirring at room temperature. The polymeric composite nanofibers were washed again with distilled water and then dried at 50 °C overnight. The regenerated composite nanofibers were reused in the batch experiment to evaluate its efficiency after the regeneration process. The adsorption-desorption cycle was repeated five times. The data demonstrate the ability of M-6 composite nanofibers to reuse after three times where the removal efficiency decreased to 54.12% as shown in Fig. 14. This regeneration ability of M-6 composite nanofibers was due to its durability as a result of its high tensile strength.

Conclusions

Nanomagnetic ZnO was successfully immobilized into PVA/Alg/CS polymeric composite nanofibers using the electrospinning technique. The fabricated composit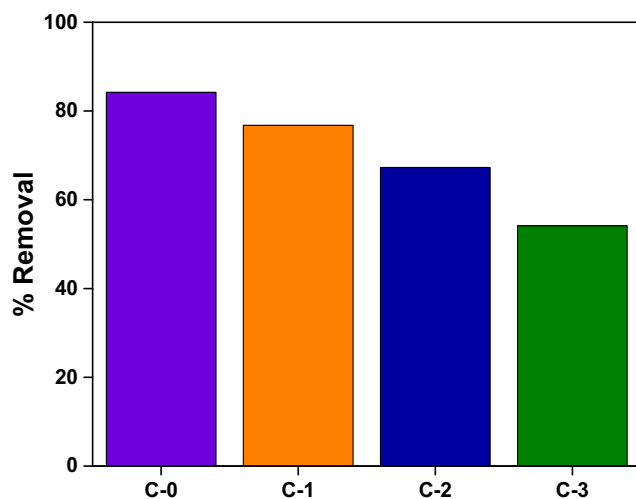e nanofibers were characterized using FTIR, XRD, VSM, SEM, AFM, TGA, tensile, and contact angle. Both the composite nanofiber dosage and phenol solution temperature have positive impacts on the phenol adsorption process. The thermodynamic parameters confirmed the endothermic and spontaneous nature of the phenol decontamination process onto the polymeric composite nanofibers. Moreover, the positive value of $\Delta S°$ indicates the increment in the randomness of the solid/solution interface in the sorption process. Furthermore, the mathematical equilibrium description of the phenol adsorption onto M-6 composite nanofibers was fitted using the Freundlich model. These mathematical equilibrium models supposed that the multilayer adsorption of phenol onto the M-6 composite nanofibers contains a physical adsorption process. Finally, the adsorption of phenol onto the prepared M-6 composite nanofibers was well described by the pseudo-second-order and intraparticle diffusion kinetic models, which demonstrate the physical adsorption process. The fabricated M-6 composite nanofiber illustrates its validity for reuse after three cycles of regenerations.

Compliance with ethical standards

Competing interests The authors declare that they have no competing interests.

Fig. 14 Recyclability test of M-6 composite nanofibers toward phenol removal

References

Abd El-Latif M, Elkady M (2011) Kinetics study and thermodynamic behavior for removing cesium, cobalt and nickel ions from aqueous solution using nano-zirconium vanadate ion exchanger. Desalination 271:41–54

Abdolmaleki AY, Zilouei H, Khorasani SN (2018) Characterization of electrospinning parameters of chitosan/poly(vinyl alcohol) nanofibers to remove phenol via response surface methodology. Polym Sci 4:1–9

Ahmed R, Tariq M, Ali I, Asghar R, Khanam PN, Augustine R, Hasan A (2018) Novel electrospun chitosan/polyvinyl alcohol/zinc oxide nanofibrous mats with antibacterial and antioxidant properties for diabetic wound healing. Int J Biol Macromol 120:385–393

Alakanandana A, Subrahmanyam A, Kumar JS (2016) Structural and electrical conductivity studies of pure PVA and PVA doped with succinic acid polymer electrolyte system. Materials Today: Proceedings 3:3680–3688

Alizadeh B, Delnavaz M, Shakeri A (2018) Removal of Cd ( ) and phenol using novel cross-linked magnetic EDTA/chitosan/TiO$_2$ nanocomposite. Carbohydr Polym 181:675–683

Alkaram UF, Mukhlis AA, Al-Dujaili AH (2009) The removal of phenol from aqueous solutions by adsorption using surfactant-modified bentonite and kaolinite. J Hazard Mater 169:324–332

Amer WA, Omran MM, Rehab AF, Ayad MM (2018) Acid green crystal-based in situ synthesis of polyaniline hollow nanotubes for the adsorption of anionic and cationic dyes. RSC Adv 8:22536–22545

Anitha A, Sowmya S, Kumar PS, Deepthi S, Chennazhi K, Ehrlich H, Tsurkan M, Jayakumar R (2014) Chitin and chitosan in selected biomedical applications. Prog Polym Sci 39:1644–1667

Anžlovar A, Orel ZC, Kogej K, Žigon M (2012) Polyol-mediated synthesis of zinc oxide nanorods and nanocomposites with poly (methyl methacrylate). J Nanomater 2012:31

Ayad MM, Salahuddin NA, Minisy IM, Amer WA (2014) Chitosan/ polyaniline nanofibers coating on the quartz crystal microbalance electrode for gas sensing. Sensors Actuators B Chem 202:144–153

Ayad MM, Amer WA, Kotp MG (2017a) Magnetic polyaniline-chitosan nanocomposite decorated with palladium nanoparticles for enhanced catalytic reduction of 4-nitrophenol. Mol Catal 439:72–80

Ayad MM, Amer WA, Kotp MG, Minisy IM, Rehab AF, Kopecký D, Fitl P (2017b) Synthesis of silver-anchored polyaniline–chitosan magnetic nanocomposite: a smart system for catalysis. RSC Adv 7:18553–18560

Ayad MM, Amer WA, Zaghlol S, Minisy IM, Bober P, Stejskal J (2018) Polypyrrole-coated cotton textile as adsorbent of methylene blue dye. Chem Pap 72:1605–1618

Babuponnusami A, Muthukumar K (2012) Removal of phenol by heterogenous photo electro Fenton-like process using nano-zero valent iron. Sep Purif Technol 98:130–135

Barbusiński K, Salwiczek S, Paszewska A (2016) The use of chitosan for removing selected pollutants from water and wastewater—short review. Architect Civ Eng Environ 9:107–115

Beheshti, H., Irani, M., Hosseini, L., Rahimi, A. and Aliabadi, M. (2016) Removal of Cr (VI) from aqueous solutions using chitosan/ MWCNT/Fe3O4 composite nanofibers-batch and column studies. Chemical Engineering Journal 284:557–564

Chandra, V., Park, J., Chun, Y., Lee, J.W., Hwang, I.-C. and Kim, K.S. (2010) Water-dispersible magnetite-reduced graphene oxide composites for arsenic removal. ACS nano 4(7):3979–3986

Chang J-J, Lee Y-H, Wu M-H, Yang M-C, Chien C-T (2012) Preparation of electrospun alginate fibers with chitosan sheath. Carbohydr Polym 87:2357–2361

Chauhan, D., Dwivedi, J. and Sankararamakrishnan, N. (2014) Novel chitosan/PVA/zerovalent iron biopolymeric nanofibers with enhanced arsenic removal applications. Environmental Science and Pollution Research 21(15):9430–9442

Chen, C.-C. and Chung, Y.-C. (2006) Arsenic removal using a biopolymer chitosan sorbent. Journal of Environmental Science and Health, Part A 41(4):645–658

Cornell RM, Schwertmann U (2003) The iron oxides: structure, properties, reactions, occurrences and uses. Wiley

Dersch R, Steinhart M, Boudriot U, Greiner A, Wendorff J (2005) Nanoprocessing of polymers: applications in medicine, sensors, catalysis, photonics. Polym Adv Technol 16:276–282

Du J, Sun B, Zhang J, Guan X (2012) Parabola-like shaped pH-rate profile for phenols oxidation by aqueous permanganate. Environ Sci Technol 46:8860–8867

El-Aassar M, El-Kady M, Hassan HS, Al-Deyab SS (2016) Synthesis and characterization of surface modified electrospun poly (acrylonitrile-co-styrene) nanofibers for dye decolorization. J Taiwan Inst Chem Eng 58:274–282

El-Ashtoukhy E, El-Taweel Y, Abdelwahab O, Nassef E (2013) Treatment of petrochemical wastewater containing phenolic compounds by electrocoagulation using a fixed bed electrochemical reactor. Int J Electrochem Sci 8:1534–1550

Elkady MF, Shokry Hassan H (2015) Equilibrium and dynamic profiles of azo dye sorption onto innovative nano-zinc oxide biocomposite. Curr Nanosci 11:805–814

Elkady M, Shokry Hassan H, El-Sayed EM (2015) Basic violet decolourization using alginate immobilized nanozirconium tungestovanadate matrix as cation exchanger. J Chemother:2015

Elkady M, Shokry Hassan H, Salama E (2016a) Sorption profile of phosphorus ions onto ZnO nanorods synthesized via sonic technique. J Eng:2016

Elkady MF, El-Aassar MR, Hassan HS (2016b) Adsorption profile of basic dye onto novel fabricated carboxylated functionalized copolymer nanofibers. Polymers 8:177

Elkady M, Hassan H, Amer W, Salama E, Algarni H, Shaaban E (2017) Novel magnetic zinc oxide nanotubes for phenol adsorption: mechanism modeling. Materials 10:1355

Elkady M, Shokry H, Hamad H (2018) Microwave-assisted synthesis of magnetic hydroxyapatite for removal of heavy metals from groundwater. Chem Eng Technol 41:553–562

Elzain AA, El-Aassar M, Hashem F, Mohamed F, Ali AS (2019) Removal of methylene dye using composites of poly (styrene-co-acrylonitrile) nanofibers impregnated with adsorbent materials. J Mol Liq 291:111335

Farrokhi M, Hosseini S-C, Yang J-K, Shirzad-Siboni M (2014) Application of ZnO–Fe3O4 nanocomposite on the removal of azo dye from aqueous solutions: kinetics and equilibrium studies. Water Air Soil Pollut 225:2113

Frenot A, Chronakis IS (2003) Polymer nanofibers assembled by electrospinning. Curr Opin Colloid Interface Sci 8:64–75

Gokila S, Gomathi T, Sudha P, Anil S (2017) Removal of the heavy metal ion chromiuim (VI) using chitosan and alginate nanocomposites. Int J Biol Macromol 104:1459–1468

Gupta, A., Chauhan, V.S. and Sankararamakrishnan, N. (2009) Preparation and evaluation of iron–chitosan composites for removal of As (III) and As (V) from arsenic contaminated real life groundwater. Water research 43(15):3862–3870

Gutha Y, Pathak JL, Zhang W, Zhang Y, Jiao X (2017) Antibacterial and wound healing properties of chitosan/poly (vinyl alcohol)/zinc oxide beads (CS/PVA/ZnO). Int J Biol Macromol 103:234–241

Hafez EE, Hassan HS, Elkady M, Salama E (2014) Assessment of antibacterial activity for synthesized zinc oxide nanorods against plant pathogenic strains. Int J Sci Technol Res 3:318–324

Han J, Tao F-M (2006) Correlations and predictions of p K a values of fluorophenols and bromophenols using hydrogen-bonded complexes with ammonia. J Phys Chem A 110:257–263

Hayat K, Gondal M, Khaled MM, Ahmed S, Shemsi AM (2011) Nano ZnO synthesis by modified sol gel method and its application in heterogeneous photocatalytic removal of phenol from water. Appl Catal A Gen 393:122–129

Huang Z-M, Zhang Y-Z, Kotaki M, Ramakrishna S (2003) A review on polymer nanofibers by electrospinning and their applications in nanocomposites. Compos Sci Technol 63:2223–2253

Islam MS, Karim MR (2010) Fabrication and characterization of poly (vinyl alcohol)/alginate blend nanofibers by electrospinning method. Colloids Surf A Physicochem Eng Asp 366:135–140

Jalayeri H, Ardejani FD, Marandi R (2013) Biodegradation of phenol from a synthetic aqueous system using acclimatized activated sludge. Arab J Geosci 6:3847–3852

Jana S, Trivedi MK, Tallapragada RM, Branton A, Trivedi D, Nayak G, Mishra R (2015) Characterization of physicochemical and thermal properties of chitosan and sodium alginate after biofield treatment. Pharm Anal Acta 6:1–9

Jayaraman K, Kotaki M, Zhang Y, Mo X, Ramakrishna S (2004) Recent advances in polymer nanofibers. J Nanosci Nanotechnol 4:52–65

Ji W, Sun Y, Yang F, van den Beucken JJ, Fan M, Chen Z, Jansen JA (2011) Bioactive electrospun scaffolds delivering growth factors and genes for tissue engineering applications. Pharm Res 28: 1259–1272

Jiao X, Gutha Y, Zhang W (2017) Application of chitosan/poly (vinyl alcohol)/CuO (CS/PVA/CuO) beads as an adsorbent material for the

removal of Pb (II) from aqueous environment. Colloids Surf B: Biointerfaces 149:184–195

Karim MR (2013) Fabrication of electrospun aligned nanofibers from conducting polyaniline copolymer/polyvinyl alcohol/chitosan oligossacaride in aqueous solutions. Synth Met 178:34–37

Khan MQ, Kharaghani D, Ullah S, Waqas M, Abbasi AMR, Saito Y, Zhu C, Kim IS (2018) Self-cleaning properties of electrospun PVA/TiO2 and PVA/ZnO nanofibers composites. Nanomaterials 8:644

Kimmer D, Slobodian P, Petráš D, Zatloukal M, Olejník R, Sáha P (2009) Polyurethane/multiwalled carbon nanotube nanowebs prepared by an electrospinning process. J Appl Polym Sci 111:2711–2714

Kumar H, Rani R (2013) Structural and optical characterization of ZnO nanoparticles synthesized by microemulsion route. Int Lett Chem Phys Astron 14:26–36

Kumar NS, Suguna M, Subbaiah MV, Reddy AS, Kumar NP, Krishnaiah A (2010) Adsorption of phenolic compounds from aqueous solutions onto chitosan-coated perlite beads as biosorbent. Ind Eng Chem Res 49:9238–9247

Kumaraswamy S, Babaladimath G, Badalamoole V, Mallaiah SH (2017) Gamma irradiation synthesis and in vitro drug release studies of ZnO/PVA hydrogel nanocomposites. Aml:546–552

Lee KY, Jeong L, Kang YO, Lee SJ, Park WH (2009) Electrospinning of polysaccharides for regenerative medicine. Adv Drug Deliv Rev 61: 1020–1032

Li D, Xia Y (2004) Electrospinning of nanofibers: reinventing the wheel? Adv Mater 16:1151–1170

Liu F, Yi B, Xing D, Yu J, Zhang H (2003) Nafion/PTFE composite membranes for fuel cell applications. J Membr Sci 212:213–223

Lu H, Wang J, Stoller M, Wang T, Bao Y, Hao H (2016) An overview of nanomaterials for water and wastewater treatment. Adv Mater Sci Eng 2016:1–10

Ma J, Zhang M, Jiang Z, Nie M, Liu G (2010) Facile fabrication of structurally stable hyaluronic acid-based composite membranes inspired by bioadhesion. J Membr Sci 364:290–297

Malayeri HZ, Ayati B, Ganjidoust H (2014) Photocatalytic phenol degradation by immobilized nano ZnO: intermediates & key operating parameters. Water Environ Res 86:771–778

Mekonnen MM, Hoekstra AY (2016) Four billion people facing severe water scarcity. Sci Adv 2:e1500323

Mohy-Eldin M, Elkady M, Abu-Saied M, Rahman AA, Soliman E, Elzatahry A, Youssef M (2010) Removal of cadmium ions from synthetic aqueous solutions with a novel nanosulfonated poly (glycidyl methacrylate) cation exchanger: kinetic and equilibrium studies. J Appl Polym Sci 118:3111–3122

Mukherjee R, De S (2014) Adsorptive removal of phenolic compounds using cellulose acetate phthalate–alumina nanoparticle mixed matrix membrane. J Hazard Mater 265:8–19

Najafabadi, H.H., Irani, M., Rad, L.R., Haratameh, A.H. and Haririan, I. (2015) Removal of Cu2+, Pb2+ and Cr6+ from aqueous solutions using a chitosan/graphene oxide composite nanofibrous adsorbent. RSC Advances 5(21):16532–16539

Namasivayam C, Sureshkumar MV (2008) Removal of chromium(VI) from water and wastewater using surfactant modified coconut coir pith as a biosorbent. Bioresour Technol 99:2218–2225

Nechita P (2017) Applications of chitosan in wastewater treatment. Biol Act Appl Mar Polysaccharides 209

Ngo HH, Guo W, Zhang J, Liang S, Ton-That C, Zhang X (2015) Typical low cost biosorbents for adsorptive removal of specific organic pollutants from water. Bioresour Technol 182:353–363

Ozkaya B (2007) Adsorption and desorption of phenol on activated carbon and a comparison of isotherm models. J Hazard Mater 129:158–163

Parida K, Pradhan AC (2010) Removal of phenolic compounds from aqueous solutions by adsorption onto manganese nodule leached residue. J Hazard Mater 173:758–764

Park JY, Patel D, Choi ES, Baek MJ, Chang Y, Kim TJ, Lee GH (2010) Salt effects on the physical properties of magnetite nanoparticles synthesized at different NaCl concentrations. Colloids Surf A Physicochem Eng Asp 367:41–46

Park H-S, Koduru JR, Choo K-H, Lee B (2015) Activated carbons impregnated with iron oxide nanoparticles for enhanced removal of bisphenol A and natural organic matter. J Hazard Mater 286:315–324

Pascariu P, Airinei A, Asandulesa M, Rotaru A (2018) Insights into the optical, magnetic and dielectric properties of some novel polysulfone/NiFe2O4 composite materials. Polym Int 67:1313–1324

Pedro-Monzonís M, Solera A, Ferrer J, Estrela T, Paredes-Arquiola J (2015) A review of water scarcity and drought indexes in water resources planning and management. J Hydrol 527:482–493

Peña-Reyes V, Marin-Bustamante M, Manzo-Robledo A, Chanona-Pérez J, Cásarez-Santiago R, Suarez-Najera E (2017) Effect of crosslinking of alginate/Pva and chitosan/Pva, reinforced with cellulose nanoparticles obtained from Agave atrovirens Karw. Procedia Eng 200:434–439

Persano L, Camposeo A, Tekmen C, Pisignano D (2013) Industrial upscaling of electrospinning and applications of polymer nanofibers: a review. Macromol Mater Eng 298:504–520

Rahmanian N, Jafari SM, Galanakis CM (2014) Recovery and removal of phenolic compounds from olive mill wastewater. J Am Oil Chem Soc 91:1–18

Ramakrishna S (2005) An introduction to electrospinning and nanofibers. World Scientific

Roy AS, Gupta S, Sindhu S, Parveen A, Ramamurthy PC (2013) Dielectric properties of novel PVA/ZnO hybrid nanocomposite films. Compos Part B 47:314–319

Salari M, Dehghani MH, Azari A, Motevalli MD, Shabanloo A, Ali I (2019) High performance removal of phenol from aqueous solution by magnetic chitosan based on response surface methodology and genetic algorithm. J Mol Liq 285:146–157

Sargazi G, Afzali D, Mostafavi A, Shadman A, Rezaee B, Zarrintaj P, Saeb MR, Ramakrishna S, Mozafari M (2019) Chitosan/polyvinyl alcohol nanofibrous membranes: towards green super-adsorbents for toxic gases. Heliyon 5:e01527

Shokry Hassan H (2019) Role of preparation technique in the morphological structures of innovative nano-cation exchange. J Mater Res Technol 8:2854–2864

Shokry Hassan H, Kashyout A, Morsi I, Nasser A, Abuklill H (2015) Development of polypyrrole coated copper nanowires for gas sensor application. Sens Bio-sensing Res 5:50–54

Shokry Hassan H, Elkady M, Farghali A, Salem AM, Abd El-Hamid A (2017a) Fabrication of novel magnetic zinc oxide cellulose acetate hybrid nano-fiber to be utilized for phenol decontamination. J Taiwan Inst Chem Eng 78:307–316

Shokry Hassan H, Elkady MF, Hafez EE, Salama E (2017b) Novel antibacterial zinc oxide polymeric nanocomposite membrane as wound dress. Nanosci Nanotechnol Asia 7:62–72

Shokry H, Elkady M, Salama E (2020) Eco-friendly magnetic activated carbon nano-hybrid for facile oil spills separation. Sci Rep 10:1–17

Sill TJ, von Recum HA (2008) Electrospinning: applications in drug delivery and tissue engineering. Biomaterials 29:1989–2006

Siva Kumar N, Subba Reddy A, Boddu VM, Krishnaiah A (2009) Development of chitosan-alginate based biosorbent for the removal of p-chlorophenol from aqueous medium. Toxicol Environ Chem 91:1035–1054

Subbiah T, Bhat GS, Tock RW, Parameswaran S, Ramkumar SS (2005) Electrospinning of nanofibers. J Appl Polym Sci 96:557–569

Sun X, Uyama H (2013) A poly (vinyl alcohol)/sodium alginate blend monolith with nanoscale porous structure. Nanoscale Res Lett 8:411

Tasic Z, Gupta V, Antonijevic M (2014) The mechanism and kinetics of degradation of phenolics in wastewaters using electrochemical oxidation. Int J Electrochem Sci 9:3473–3490

Thinakaran N, Baskaralingam P, Pulikesi M, Panneerselvam P, Sivanesan S (2008) Removal of Acid Violet 17 from aqueous solutions by adsorption onto activated carbon prepared from sunflower seed hull. J Hazard Mater 151:316–322

Üner O, Geçgel Ü, Bayrak Y (2016) Adsorption of methylene blue by an efficient activated carbon prepared from Citrullus lanatus rind: kinetic, isotherm, thermodynamic, and mechanism analysis. Water Air Soil Pollut 227:247

Vijayalakshmi P, Bala VSS, Thiruvengadaravi K, Panneerselvam P, Palanichamy M, Sivanesan S (2010) Removal of acid violet 17 from aqueous solutions by adsorption onto activated carbon prepared from pistachio nut shell. Sep Sci Technol 46:155–163

Voronova MI, Surov OV, Guseinov SS, Barannikov VP, Zakharov AG (2015) Thermal stability of polyvinyl alcohol/nanocrystalline cellulose composites. Carbohydr Polym 130:440–447

Wang X, Fu Q, Wang X, Si Y, Yu J, Wang X, Ding B (2015) In situ cross-linked and highly carboxylated poly (vinyl alcohol) nanofibrous membranes for efficient adsorption of proteins. J Mater Chem B 3:7281–7290

Yamasaki H, Makihata Y, Fukunaga K (2006) Efficient phenol removal of wastewater from phenolic resin plants using crosslinked cyclodextrin particles. J Chem Technol Biotechnol 81:1271–1276

Yang X, Shao C, Guan H, Li X, Gong J (2004) Preparation and characterization of ZnO nanofibers by using electrospun PVA/zinc acetate composite fiber as precursor. Inorg Chem Commun 7:176–178

Yin J, Deng B (2015) Polymer-matrix nanocomposite membranes for water treatment. J Membr Sci 479:256–275

Zhao J, Ma J, Chen J, Pan F, Jiang Z (2011) Experimental and molecular simulation investigations on interfacial characteristics of gelatin/polyacrylonitrile composite pervaporation membrane. Chem Eng J 178:1–7

Zheng L, Su W, Qi Z, Xu Y, Zhou M, Xie Y (2011) First-order metal–insulator transition and infrared identification of shape-controlled magnetite nanocrystals. Nanotechnology 22:485706